
Study of Structural and Magnetic Properties for Hybrid Compounds of " $X(\text{SrFe}_{12}\text{O}_{19}) + (1-X) (\text{BiFeO}_3)$ "

Pedro Antonio Marinho-Castellanos^{1,*}, Arles Vega-Garcia¹, Julio Cesar Velazquez-Infante²,
Yadira Marinho-Del Toro³, Braddy Ivan Jimenez-Morales^{4,5}, Joaquin Matilla-Arias⁶

¹Department of Physics, University of Holguin, Holguin, Cuba

²Arid Agroecosystem Studies Center, University of Holguin, Holguin, Cuba

³Minagri Training and Overcoming Center, Santiago de Cuba, Cuba

⁴Physics Institute, Kazan Federal University, Kazan, Russian Federation

⁵Department of Physics, University of Camagüey, Camagüey, Cuba

⁶Department of Basic Sciences and Applied Informatics, University of Granma, Granma, Cuba

Email address:

pamarcast@uho.edu.cu (P. A. Marinho-Castellanos)

*Corresponding author

To cite this article:

Pedro Antonio Marinho-Castellanos, Arles Vega-Garcia, Julio Cesar Velazquez-Infante, Yadira Marinho-Del Toro, Braddy Ivan Jimenez-Morales, Joaquin Matilla-Arias. Study of Structural and Magnetic Properties for Hybrid Compounds of " $X(\text{SrFe}_{12}\text{O}_{19}) + (1-X) (\text{BiFeO}_3)$ ". *Engineering Science*. Vol. 5, No. 1, 2020, pp. 5-9. doi: 10.11648/j.es.20200501.12

Received: January 29, 2020; **Accepted:** February 10, 2020; **Published:** May 28, 2020

Abstract: A structural and magnetic study of the system $X(\text{SrFe}_{12}\text{O}_{19}) + (1-X) (\text{BiFeO}_3)$ with $X=0, 0.20, 0.40, 0.50, 0.60, 0.80$ and 1.0 is presented in this work. The individual phases were obtained by the Sol-Gel method. The powders were mixed by mechanical grinding, then pressed and sintered. Experimental techniques of X-ray diffraction and vibrational magnetometry were used for the characterization of the samples and the Hanawalt method and the Match! Phase Identification from Powder Diffraction were used for the qualitative determination of the phases present in each sample. Rietveld's analysis was carried out with the FullProf Suite-2008 program. The structural results obtained show slight variations of the crystal lattice parameters for both phases and the coexistence of both phases in each sample. The magnetic characterization shows a linear increase of the saturation magnetization, the remanent magnetization and the magnetic anisotropy constant K_1 , as a function of the concentration of the BiFeO_3 and $\text{SrFe}_{12}\text{O}_{19}$ phases. A satisfactory congruence is observed between the theoretical predictions and the experimental measurements, an indication that the magnetic parameters reported are due to the superposition, in each compound, of their individual values. Both the XRD pattern and the structural and magnetic characterization show that the two phases coexist individually in the matrix and have a good chemical compatibility between them.

Keywords: Sol-Gel Methods, Magnetic Properties, Hexaferrite, Theoretical Predictions, Rietveld Refinement

1. Introduction

In the last two decades, hybrid materials have received a growing boost in research, since they normally provide a new multi-functional material with different or complementary physical properties to each constituent, which were not present in their individual components, and can provide new or improved properties for various applications [1].

M-type hexagonal ferrites have attracted much attention for their excellent magnetic properties and potential applications in various fields of industry and technology at

present [2]. The most important of these magneto-hard materials, from the practical point of view, are barium ferrites ($\text{BaFe}_{12}\text{O}_{19}$) and strontium ferrites ($\text{SrFe}_{12}\text{O}_{19}$ (SrM)) for their suitable values of saturation magnetization, remanent magnetization and high coercive force [1-4]. On the other hand, it has been observed the simultaneous occurrence of a large ferroelectricity and a strong ferromagnetism in the hexagonal strontium ceramics ($\text{SrFe}_{12}\text{O}_{19}$) [5].

Likewise, the distorted perovskite structure of the simple phase of BiFeO_3 is one of the most representative multiferroics and it is of great importance due to its

antiferromagnetic and ferroelectric behavior [6-8].

The contribution of two phases in equilibrium, such as a ferrite and a ferroelectric, form a hybrid compound, which can give rise to a multiferroic material. Currently these are investigated due to their potential applications such as; transducers, sensors, data storage, interrupt devices, etc. [6, 9].

Therefore, the preparation of a material in which a large ferroelectricity and a strong ferrimagnetism coexist at room temperature, could be a milestone for modern electricity and the development of functional materials [5]. Furthermore, the compounds, of the type mentioned above, allow a variation of some of their properties (for example, the magnetic ones) that are not possible in the material in its simple phase and can give rise to new or improved properties for various applications [4].

Very few works have been published on nanocompounds of the type $X(\text{MFe}_{12}\text{O}_{19}) + (1-X)(\text{BiFeO}_3)$ with M=Ba, Sr, studying their morphological, magnetic and electrical properties, opening a new direction of research as a multiferroic candidate using oxides of hexagonal ferrites type M [2].

In addition, this material can also behave like a hybrid since it is a biphasic compound formed by a strong ferrimagnetic ($\text{SrFe}_{12}\text{O}_{19}$) and a weak ferromagnetic (BiFeO_3). In this sense the system $X(\text{SrFe}_{12}\text{O}_{19}) + (1-X)(\text{BiFeO}_3)$ they have been very little investigated.

In the present work, phases of BiFeO_3 and $\text{SrFe}_{12}\text{O}_{19}$ are obtained by the Sol-Gel method, subsequently mixing them to give rise to a series of compounds of the type $X(\text{SrFe}_{12}\text{O}_{19}) + (1-X)(\text{BiFeO}_3)$ such that X=0, 0.2, 0.4, 0.5, 0.6, 0.8, and 1.

The study of the variations of some structural and magnetic properties, as well as the correlation between their theoretical and experimental magnetic predictions as a function of the concentration of each one of the phases is the objective of this work and its scientific novelty.

2. Materials and Methods

2.1. Obtaining the Initial Phases and the Compounds

To obtain the BiFeO_3 and $\text{SrFe}_{12}\text{O}_{19}$ phases by the Sol-Gel method, the nitrates of the corresponding metals, with purities higher than 99%, were used. The primary nitrates were dissolved in deionized water in a 1:2 ratio. Citric acid was also dissolved in deionized water. All solutions were placed separately on ultrasound for 30 minutes. All the solutions corresponding to each phase were mixed. The molar ratio between nitrates and citric acid is 1: 1. Then an aqueous solution of ammonium hydroxide was added until reaching a PH=7 each. Both mixtures were placed in ultrasound for 30 minutes at a temperature of 70°C. Later they were left to stand at room temperature for 36 hours (gel aging process). Each phase was heated to 120°C, under stirring, until obtaining the dry gel. Hence the dry gel of the BiFeO_3 ferrite was pre-calcined at 450°C for 5 hours and then calcined at 1000°C for 2 hours. The $\text{SrFe}_{12}\text{O}_{19}$ phase

was pre-calcined at 700°C for 5 hours and then calcined at 1100°C for 2 hours. In both cases the heating rate of the oven was 4°C/min.

To obtain each of the hybrid compounds, the phases were weighed, mixed and ground in a ball mill for 3 hours. Subsequently, 3 drops per gram of weight of polyvinyl alcohol (PVA) were added as binder, each compound was pressed in a cylindrical matrix of 13 mm in diameter at a pressure of 2.6 ton/cm². Finally, the tablets obtained were sintered at the optimum temperature of each compound, with a heating rate of 2°C/min for 3 hours.

2.2. Characterization of the Samples Obtained

The structural characterization was carried out from the XRD patterns obtained in a XPERT-PRO 2011 type diffractometer coupled to a Panalytical measurement system for the control of all the measurement parameters and the automatic realization of them. For the qualitative determination of the phases present in each sample, the Hanawalt method and the Match! "Phase Identification from Powder Diffraction". Rietveld's analysis was carried out with the FullProf Suite-2008 program.

The magnetic measurements were made in a Vibrating Sample Magnetometer (VSM) of the Versalab-Quantum Design type, model MPMS-5 with a high-tech instrumentation system and SQUID sensor. The initial magnetization curves from 0 to 25 KOe and the hysteresis loops from -25 to 25 KOe were measured.

Of the referred magnetic measurements were found the values of the remanent magnetization (M_{rem}), the saturation magnetization (M_{sat}), the ratio ($M_{\text{rem}}/M_{\text{sat}}$) and the magnetic anisotropy constant (K_1) were determined.

3. Magnetic Predictions

Calculations of predicted magnetic parameters

$$M_{\text{sat}_{\text{pred}}} = XM_{\text{sat}_{\text{SrM}}} + (1 - X)M_{\text{sat}_{\text{BiFeO}_3}} \quad (1)$$

Where M_{sat} is the saturation magnetization; predicted according to the calculation of saturation magnetization based on the number of cations per sites and the magnetic moment of the Fe^{3+} cation [10-13], for the SrM and the BiFeO_3 respectively and X is the concentration of the SrM phase in the compound.

$$M_{\text{rem}_{\text{pred}}} = XM_{\text{rem}_{\text{SrM}}} + (1 - X)M_{\text{rem}_{\text{BiFeO}_3}} \quad (2)$$

Where M_{rem} is the remanent magnetization predicted for the SrM [14] and the BiFeO_3 respectively [15].

$$K_{1_{\text{pred}}} = XK_{1_{\text{SrM}}} + (1 - X)K_{1_{\text{BiFeO}_3}} \quad (3)$$

Where K_1 is the effective anisotropy constant; predicted according to the calculation of this parameter for the SrM and the BiFeO_3 respectively, using the expression taken from [16].

4. Results and Discussion

4.1. Structural Characterization

The refined x-ray diffraction patterns corresponding to each compound of the system under study are presented in figure 1, with the intensities calculated during the refinement by the Rietveld method, the difference between the observed and calculated intensities and the Bragg positions. for the two initial phases of the system.

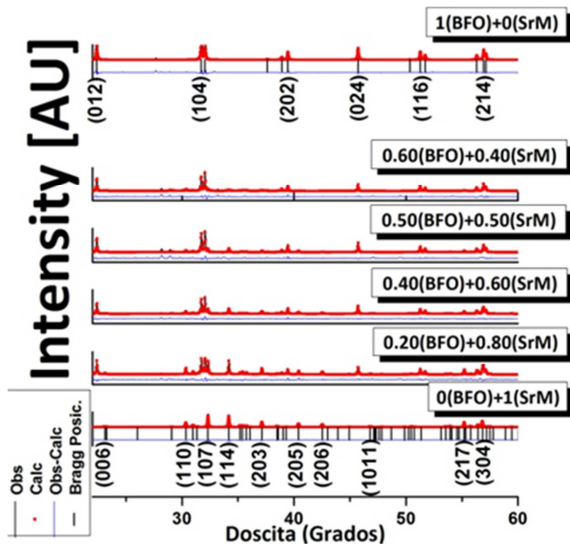


Figure 1. Fraction of the x-ray diffraction pattern as a function of 2θ ($23^\circ < 2\theta \leq 60^\circ$), using the concentration of each particular phase as a parameter. The Bragg positions and the Miller index of each component have been included.

This figure shows that the main reflections of the $BiFeO_3$ phase are present for all the biphasic compounds. This is explained by the high value of the atomic number of bismuth in this phase. The intensity of each reflection, for this phase, decreases with the concentration in the compounds.

Figure 2 shows the dependence of the crystal lattice parameter, "a" with the concentration of each individual phase.

In the case of strontium ferrite the parameter "a" has a maximum value for $X=0.2$, remaining approximately constant for $X > 0.2$. This is explained due to a greater breakdown of the original cells of this phase for very small concentrations during the grinding process.

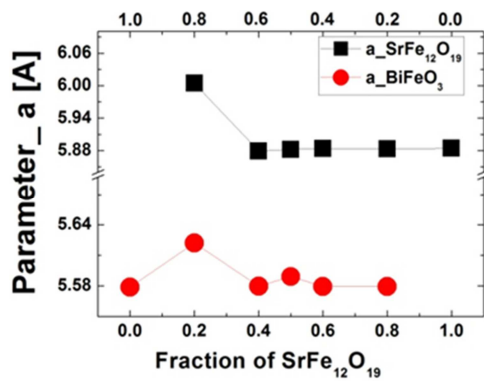


Figure 2. Parameter "a" of the lattice as a function of 2θ using the concentration of each individual phase as a parameter.

For the other initial phase ($BiFeO_3$) the behavior of the parameter "a" has a maximum in $(1 - X)=0.8$ due to the large number of grains that participate in the grinding process, without amorphization of the matrix, causing the displacement of crystallographic sites that on average increase the crystal lattice parameter "a". From there, the behavior is approximately constant.

In the case of the parameter "c" for the pure phase of SrM (Figure 3), the behavior is the same as for the parameter "a" but the effect is smaller because these cells are hexagonal and grow in the direction [001].

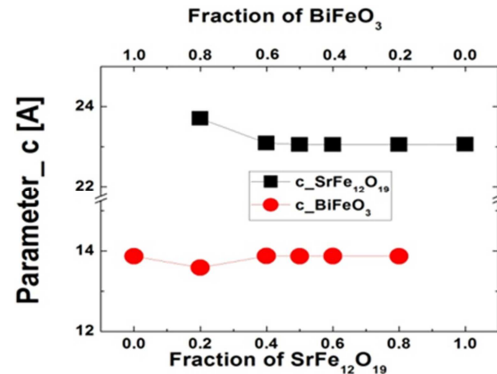


Figure 3. Parameter "c" of the crystal lattice as a function of 2θ using the concentration of each individual phase as a parameter.

The parameter "c" for the phase of $BiFeO_3$ has a minimum in $(1 - X)=0.8$, being practically constant from there, a result consistent with what is proposed for the parameter "a".

4.2. Magnetic Characterization

Figure 4 shows how the magnetization of each compound increases with the increase of the concentration of the $SrFe_{12}O_{19}$ phase, because the magnetization of the compound as a whole depends, basically, on the heavy sum of the magnetizations of the phases that compose matrix. It is also evident that for $0.4 \leq X$, the $BiFeO_3$ phase predominates in the dependence of these curves, modulated by the contribution of the $SrFe_{12}O_{19}$ phase to the total magnetization of the compound.

For $X \geq 0.5$ the opposite happens, the form of the dependence is governed by the SrM modulated by the contribution of the BFO phase.

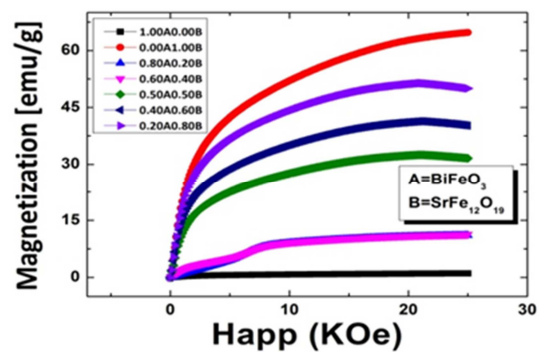


Figure 4. Curves of initial magnetization according to the intensity of the applied magnetic field (H_{app}). The concentration of each individual phase has been taken as a parameter.

The tendency to decrease magnetization for $X=0.40$ and 0.20 is due to the fact that at these field values the SrM is saturated and the contribution of the BFO phase is small.

Figure 5 reports the magnetic hysteresis loops as a function of the applied magnetic field, using as a parameter the concentration of each phase for the compounds under study.

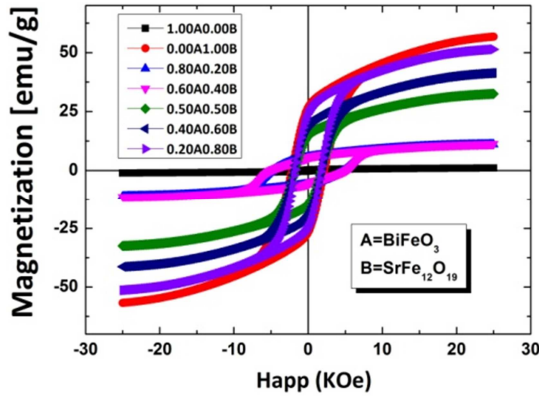


Figure 5. Magnetic hysteresis loops as a function of the intensity of the applied magnetic field (H_{app}). The concentration of each individual phase has been taken as a parameter.

The results corroborate what was said above for the dependence of the magnetization with the concentration of each phase in the matrix. Here is observed that the width of the magnetic hysteresis loop for $0.4 \leq X$ and its inclination are determined by the BFO phase and from $X \geq 0.5$ by the concentration of the SrM phase in the matrix.

Figure 6 reports the comparison between the predicted and experimental saturation magnetization as a function of the concentration of each phase in each of the analyzed compounds.

The coincidence between the predicted and the experimental curve is correct, which shows that the saturation magnetization is the superposition of the contribution of each of the phases to the saturation magnetization as a whole, according to equation (1).

For $X=0.4$ and 0.8 we can see a deviation of the linear behavior due to the tension in the crystal lattice that limits the movement of the magnetic domains.

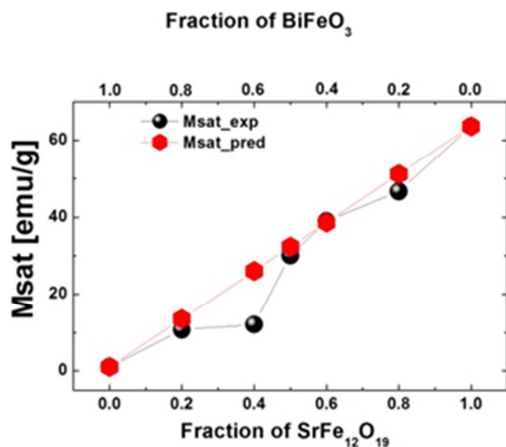


Figure 6. Comparison between the predicted and experimental saturation magnetization as a function of the concentration of each phase in each of the analyzed compounds.

Figure 7 reports the comparison between the predicted and determined remnant magnetization of the hysteresis loop as a function of the concentration of each phase in each of the compounds studied.

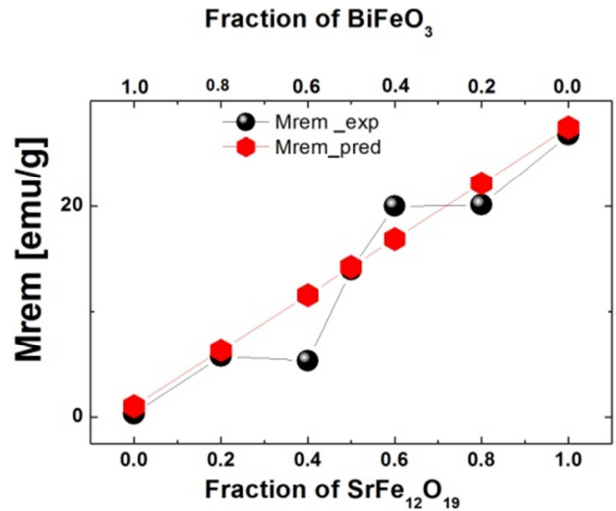


Figure 7. Comparison between the predicted and experimental remnant magnetization as a function of the concentration of each phase in each of the analyzed compounds.

The remnant magnetization is an extrinsic quantity that also depends on the shape and average size of the grains, which explains the deviation of the linearity observed for $X=0.4$ and 0.8 which corresponds to a larger grain matrix. For $X=0.6$ it indicates that the matrix is characterized by smaller and more regular grains.

The comparison between the magnetic anisotropy constant K_1 of the analyzed compounds, as a function of the concentration of each phase, is reported in Figure 8.

It is in the magnetic anisotropy constant K_1 where the variations that take place, when going from a simple phase to a compound, become evident, all of which is obvious by the change in slope of this dependence for $0.2 \leq X \leq 0.8$.

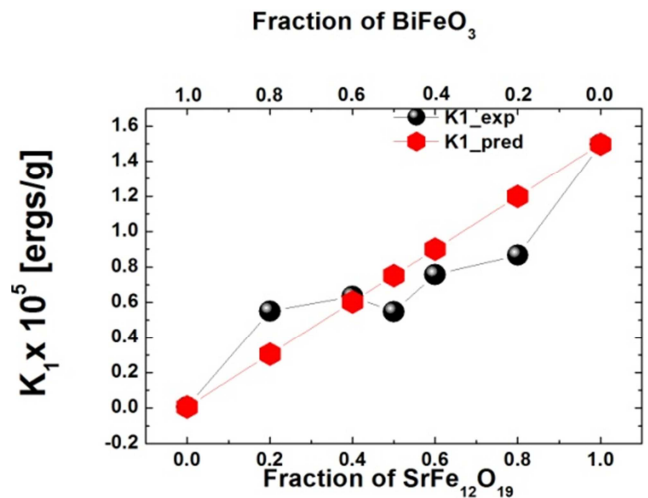


Figure 8. Comparison between the magnetic anisotropy constant K_1 of the compounds as a function of the concentration of each phase.

The figure shows, that the experimental results tend to those predicted by the expression (3). The deviations observed with respect to the theoretical curve are due to the fact that the magnetic anisotropy constant depends on the chemical composition and the structural arrangement for a wide range of grain size (Intrinsic Magnitude). It is also affected by defects and non-magnetic inclusions present in the matrix. When these defects or inclusions are small (with respect to grain size), the anisotropy constant tends to increase, as seen for $X=0.2$. For values $0.5 \leq X \leq 0.8$ the opposite take place and the magnetic anisotropy constant is lower than predicted.

5. Conclusions

It has been shown that in the first magnetization curves and the magnetic hysteresis loops for $0.4 \leq X$ the dependence of the $BiFeO_3$ phase predominates, modulated by the contribution of the $SrFe_{12}O_{19}$ to the total magnetization of the compound while for $X \geq 0.5$ the form of the dependence is governed by the SrM , but in this case, modulated by the contribution of the $BiFeO_3$. In both cases these behaviors are governed by the contribution of each phase to the magnetic properties of the compound as a whole.

In the compounds $X(SrFe_{12}O_{19}) + (1-X)(BiFeO_3)$ an appreciable range of variation of all the analyzed magnetic parameters has been reached which broadens the range of possible applications of this type of hybrid material:

$$\sim 1.56 \times 10^4 \frac{\text{erg}}{\text{g}} \leq K_1 \leq 1.45 \times 10^5 \frac{\text{erg}}{\text{g}}$$

$$\sim 0.03 \frac{\text{emu}}{\text{g}} \leq M_{sat} \leq 63.0 \frac{\text{emu}}{\text{g}}$$

$$\sim 0.02 \frac{\text{emu}}{\text{g}} \leq M_{rem} \leq 26.0 \frac{\text{emu}}{\text{g}}$$

It has become evident that the saturation magnetization, the remanent magnetization and the crystalline magneto anisotropy constant depend on the concentration of the individual phases as predicted by equations (1), (2) and (3) respectively.

References

- [1] J. Jiang, L. H. Ai; Journal of Alloys and Compounds 502 (2010) 488–490.
- [2] M. A. Ahmed, S. F. Mansour, H. Ismael; Journal of Magnetism and Magnetic Materials 378 (2015) 376–388.
- [3] A. A. Nourbakhsh, A. Vahedi, A. Nemati, M. Noorbakhsh, S. N. Mirsatari, M. Shaygan, K. J. D. Mackenzie; Ceramics Internacional 40 (2014) 5675-5680.
- [4] S. S. Ashima, R. Ashish Aganval, Monica Neetu Ahlawat; Journal of Applied Physics 112 (2012) 014110.
- [5] G. Tan, X. Chen; Journal of Electronic Materials 42 (5) (2013).
- [6] J. K. Kim, S. S. Kim, W-J. Kim; Materials Letters 59 (2005) 4006 – 4009.
- [7] A. Singh, V. Singh, K. K. Bamzai; Materials Chemistry and Physics 155 (2015) 92-98.
- [8] T-J Park, G. C. Papaefthymiou, A. J. Viescas, Y. Lee, H. Zhou, S. S. Wong; PHYSICAL REVIEW B 82 (2010) 024431.
- [9] D. Pandey, A. Singh; Bulletin Materials Science; 32 (3) (2009) 361–367.
- [10] P. A. Mariño-Castellanos, A. C. Moreno-Borges, G. OrozcoMelgar, J. A. García and E. Govea-Alcaide, Physica B: Condensed Matter 406 (2011) 3130–3136.
- [11] J. Matilla-Arias, E. Govea-Alcaide, P. Mariño-Castellanos, F. Rosales-Saiz; J Supercond Nov Magn 31 (2018) 251–256.
- [12] J. Matilla-Arias, E. Govea-Alcaide, P. Mariño-Castellanos, F. Rosales-Saiz, I. F. Machado, K. Montero-Rey, J Supercond Nov Magn (2019) 152-158.
- [13] P. A. Mariño-Castellanos, A. Vega-García, E. Fernández-Cruz, B. I. Jimenez-Morales; American Journal of Engineering and Technology Management. Vol. 4, No. 6, 2019, pp. 83-90.
- [14] M. A. Almessiere, Y. Slimani, A. D. Korkmaz, H. Gungunes, M. Nawaz, Sagar E. Shirsath, A. Baykal, I. Ercan; Journal of Sol-Gel Science and Technology (2019) 92: 239–251.
- [15] Nidhi Sheoran, Vinod Kumar, Ashok Kumar; Journal of Magnetism and Magnetic Materials 475 (2019) 30–37.
- [16] Sunita Dagar, Ashima Hooda, Satish Khasa, Meena Malik; Journal of Alloys and Compounds 806 (2019) 737-752.